Epilepsia, **47**(5):908–915, 2006
Blackwell Publishing, Inc.

Voxel-based Morphometry Reveals Excess Gray Matter Concentration in Patients with Focal Cortical Dysplasia

*†Leonardo Bonilha, ‡Maria Augusta Montenegro, †Chris Rorden, ‡Gabriela Castellano, ‡Marilisa Mantovani Guerreiro, ‡Fernando Cendes, and ‡Li Min Li

*Departments of *Neuropsychiatry and †Communication Sciences and Disorders, University of South Carolina, Columbia, South Carolina, U.S.A.; and ‡ Department of Neurology, State University of Campinas, Campinas, Brazil*

Summary: *Purpose:* Many patients with focal cortical dysplasia (FCD) continue to have seizures after surgical treatment. The usual explanation for the poor surgical outcome is the presence of residual dysplastic tissue missed by the preoperative neuroimaging investigation and therefore not resected during surgery. We apply a voxel-based morphometry (VBM) analysis to the magnetic resonance imaging (MRI) scans from patients with epilepsy and visually detected FCD to investigate whether (a) VBM is able to detect gray-matter concentration (GMC) abnormalities in patients with FCD, and (b) whether the extent of GMC abnormalities in the brain of these patients differs from the regions observed by using visual inspection.

Methods: We studied 11 patients with visually detected FCD (eight of them with histologic confirmation of FCD). The GMC from each one of these patients was compared with the mean GMC from a control group of 96 normal healthy subjects by using an optimized VBM protocol.

Results: Ten of 11 patients showed statistically significant GMC excess, and among patients with GMC excess, only one showed GMC excess that was not exactly correspondent to the visually detected FCD. Seven patients exhibited excess in GMC extending beyond the area of visually detected FCD.

Conclusions: This preliminary neuroimaging study suggests that (a) VBM can detect GMC excess in patients with FCD, and (b) GMC excess in these patients can extend to brain areas not visually defined as abnormal. Abnormal areas detected by VBM can possibly correspond to mild malformations of cortical development, supporting the notion that the surgical refractoriness observed in patients with FCD can be due to the incomplete resection of the dysplastic tissue. **Key Words:** Focal cortical dysplasia—Epilepsy—Voxel-based morphometry.

Focal cortical dysplasia (FCD) is a developmental malformation of the cerebral cortex that is now recognized as one of the leading causes of drug-resistant epilepsy (1–5). Magnetic resonance imaging (MRI) is currently the noninvasive method of choice for the in vivo diagnosis of FCD. The presence of focal cortical thickening, alterations in the sulci and gyri pattern, blurring between gray- and white-matter transition, and T_2 signal elongation of the subcortical white matter that tapers toward the ventricle are well-established criteria for the neuroimaging diagnosis of FCD (6).

Carefully designed MRI protocols can reliably detect subtle dysplastic lesions that will not be identified by routine MRI evaluation (2,7,8). Although the diagnosis of FCD has improved, its surgical treatment remains suboptimal (2,9). Optimal surgical outcome—that is, seizure freedom—is achieved in ∼50% of the patients with FCD (9,10) or different malformations of cortical development (11). The reasons that many patients do not become seizure free after epilepsy surgery are still largely unknown. One possible explanation for the poor surgical outcome in these patients is that the visually detected lesions in these patients are just the "tip of the iceberg" of a more pervasive dysplastic lesion that is not detected by visual inspection, as suggested by histologic (5, 12–16) and electrophysiologic (17) findings.

New automated brain-imaging techniques have been used to investigate subtle morphometric abnormalities that are associated with neurologic disorders. Voxel-based morphometry (VBM) is a technique that uses automatic classification of brain tissues (i.e., gray matter, white matter, and cerebrospinal fluid) and permit the calculation of the probability of a each voxel belonging to a spatially normalized image to fit into the category of a segmented tissue. VBM also can be used to compare different populations regarding their profile of distribution of segmented tissues (18). Applied to epilepsy, VBM has been successfully used to confirm atrophy that extends beyond the

Accepted January 19, 2006.
Address correspondence to Dr. L.L. Min at Department of Neurology, Faculty of Medicine, UNICAMP, 13083-970, Campinas, Brazil. E-mail: limin@fcm.unicamp.br

hippocampus in patients with temporal lobe epilepsy (19), by showing a diffuse reduction in gray-matter concentration (GMC) in areas adjacent to the hippocampus or connected to the limbic system (20,21).

The objective of this study was to quantify the GMC in a selected group of patients with drug-refractory partial epilepsy due to FCD. We compared, by using an optimized VBM protocol, the GMC of each one of these patients with the distribution of GMC in a large group of healthy individuals. One of the visual features of FCD is the increased thickness of the dysplastic cortical mantle. Thus we hypothesized that these patients might exhibit excess of GMC in the areas corresponding to the FCD. Our aims were (a) to assess whether VBM can detect excess GMC in the regions that have been visually defined as FCD, and (b) to investigate whether these patients show excess GMC in other brain areas different from the visually suspected area.

METHODS

Subjects and diagnostic protocol

We evaluated 11 consecutive patients with a neuroimaging diagnosis of FCD (3,22) (mean age, 17 ± 12 years). All patients were referred from the outpatient epilepsy clinic of our institution. The diagnosis of FCD was performed by a thorough neurologic investigation composed of a comprehensive history assessment and physical examination, interictal electroencephalograms (EEGs), and an in-house–developed protocol optimized for the visual investigation of FCD by using multiplanar and curvilinear reconstruction of high-resolution MRI films (7,8). The diagnosis of the epileptic syndrome was based on International League Against Epilepsy (ILAE) criteria (23).

Visual inspection suggested that each patient had only a single area of FCD, and no evidence of any other type of brain lesion was found. After the MRI scan, eight patients underwent surgical treatment for epilepsy by resection of the visually detected dysplastic region; all of them had histologic confirmation of FCD (22,24). We included in this study patients with one or more of the following histologic abnormalities: cortical architectural abnormalities such as dyslamination, immature neurons, giant neurons, dysmorphic neurons, and balloon cells. Not all patients showed balloon cells (i.e., not all patients belong to the category defined by Palmini et al. (22) as type IIB, which is composed of architectural abnormalities associated with dysmorphic neurons and balloon cells. Our patients belonged in category II, which has been defined as Taylor-type FCD (dysmorphic neurons without or with balloon cells) by Palmini et al. Table 1 shows the clinical information of the patients.

Control group

We evaluated 96 normal healthy volunteers recruited from the local community (44 men) with mean age of

TABLE 1. *Clinical information of the patients with focal cortical dysplasia*

Subject	Gender	Age (yr)	Age at onset of seizures	Seizure frequency	Neurologic examination	EEG	Surgical outcome	Histologic analysis	VBM abnormalities
Subject 1	M	10	5 mo	2–3 per wk	Normal	Multifocal	Refractory to seizure control	Focal cortical dysplasia	Matches visual and extends beyond
Subject 2	M	8	1 yr	Daily	Normal	Left temporoparietal	Temporary postoperative (2 yr) period of seizure freedom, currently refractory to seizure control	Focal cortical dysplasia	Matches visual and extends beyond
Subject 3	F	5	20 days	Daily	Mild left hemiparesis	Multifocal	Seizure free	Focal cortical dysplasia	Matches visual and extends beyond
Subject 4	M	15	2 yr	Daily	Normal	Left frontal	Seizures partially controlled	Focal cortical dysplasia	Matches visual and extends beyond
Subject 5	F	34	3 yr	Daily	Normal	Multifocal	Refractory to seizure control	Not surgically treated	Matches visual only
Subject 6	M	10	6 yr	Daily	Normal	Multifocal	Refractory to seizure control	Focal cortical dysplasia	Matches visual and extends beyond
Subject 7	M	8	1 yr	Daily	Normal	Multifocal	Seizure free	Focal cortical dysplasia	Matches visual and extends beyond
Subject 8	M	15	4 yr	Daily	Normal	Multifocal	Refractory to seizure control	Focal cortical dysplasia	Does not match visual
Subject 9	F	40	1 yr	Daily	Normal	Multifocal	Seizure free	Focal cortical dysplasia	Matches visual only
Subject 10	F	8	3 yr	3 per wk	Normal	Left temporal	Refractory to seizure control	Not surgically treated	Absent
Subject 11	M	36	5 mo	1 per wk	Learning disability	Multifocal	Refractory to seizure control	Not surgically treated	Matches visual and extends beyond

30.1 years (SD, 11.3 years), ranging from 9 to 66 years. The mean age of patients was significantly smaller than the mean age of controls [$t(128) = 4$; $p < 0.05$]. However, the age range in both patients and control subjects was sufficiently large to model age-related confounds in our statistical model for the VBM analyses. Therefore we included age as a covariate for our subsequent statistical analyses. Moreover, each patient was individually compared with the group of controls, and only one patient (patient 3) had an age younger than two standard deviations (SD) below the mean age of the control group. All other patients had ages that were within 2 SD of the mean age.

Electroencephalogram

Ictal or interictal EEGs were performed, and the epileptiform abnormalities were classified as either focal or multifocal. EEG data also are summarized in Table 1. Multifocal activity was defined by the presence of independent ictal or interictal epileptiform discharges in two or more different cerebral lobes. Focal abnormalities were defined by the presence of ictal and interictal epileptiform activity at only one cerebral lobe.

Voxel-based morphometry

We applied an optimized VBM protocol to assess GMC changes in these patients. VBM was performed on volumetric T_1-weighted images with either 1-mm isotropic voxels or with $1.5 \times 0.97 \times 0.97$-mm voxels. All images were acquired on the same Elscint Prestige 2 Tesla scanner (Haifa, Israel) by using a spoiled gradient-echo sequence (TR, 22 ms; TE, 9 ms; flip angle, 35 degrees; matrix, 256×220).

DICOM images were transformed into ANALYZE format by using MRIcro software (Chris Rorden, www.mricro.com) (25) and skull-stripped by using the brain-extraction tool (Steve Smith, www.fmrib.ox.ac.uk/fsl/bet/). The VBM analysis was performed by using modified routines present in the SPM2 software package (Wellcome Department of Cognitive Neurology, www.fil.ion.ucl.ac.uk) (18). A skull–stripped template and prior images of gray and white matter and CSF were created from the images from the 96 control subjects. We decided to use our own template in the analysis to overcome (a) differences in contrast from our images to the standard template used by SPM, (b) nonuniformities in image intensity and inhomogeneities in B0 field crated by our scanner, and (c) differences in the demographics of our population compared with the population used for the generation of the SPM standard template. The prior images and the template were convolved with an isotropic gaussian kernel (IGK) of 8 mm and were used for optimizing the nonlinear normalization of raw skull-stripped images. Initial spatial normalization used a 12-parameter linear transformation (translation, rotation, zoom, and shear functions). Spatial normalization was refined by using 16 nonlinear iterations, medium regularization, and a 25-mm cutoff. Spatially normalized images were resliced to an isotropic 1 mm. The images underwent segmentation of gray matter by using SPM2's built-in routines, which estimate the probability that each voxel is gray matter. The segmented images were modulated (26) to preserve the quantity of tissue (e.g., gray matter) while ensuring a good spatial alignment between patients and controls. Finally, the images were convolved with an IGK of 10 mm to minimize gyral interindividual variability. This smoothing converts maps of tissue-classification probabilities (i.e., segments) into images of local gray-matter concentration. After smoothing, the data represent the proportion of the volume under the smoothing kernel that has been classified, probabilistically, as gray matter. In addition, this smoothing renders gray-matter concentration normally distributed, enabling us to apply standard statistical parametric mapping techniques.

The normalized, segmented, modulated, and smoothed data were analyzed by using SPM2. This information corresponds to probabilistic maps of gray-matter concentration and apply exclusively to smoothed distribution of gray matter, therefore localized within GM. The resulting images were compared by using an analysis of covariance (ANCOVA) with age as a nuisance factor to search for differences in GMC between control subjects and each patient with FCD. Contrasts were defined to estimate the probability of each voxel being gray matter. This analysis included grand mean scaling and proportional threshold masking (set to 0.8) and implicit masking. This proportional threshold-masking level was chosen as we a priori expected to identify gray-matter hyperintensities (note that this threshold will eliminate regions with low GMC). We used an uncorrected statistical threshold of $p < 0.001$ ($T = 3.18$) with an extent threshold looking for clusters with ≥ 32 contiguous voxels. The determination and naming of the brain region that showed differences in GMC were performed by assessing their stereotaxic coordinates provided in the SPM output through the Internet freely available Talairach Daemon client (http://ric.uthscsa.edu/projects/talairachdaemon.html).

However, the difference in GMC observed in the subjects with FCD could be explained by the simple individual variability of sulci and gyral pattern, which can persist despite the normalization and smoothing procedures. In this case, detected increased GMC could occur by chance within the normal population and is not related to the presence of FCD. Nevertheless, VBM is based on a number of assumptions, including normality assumptions and limit distributions for the null distribution of the size and extent of regional effects. To make absolutely sure these are assumptions were not violated in our data, we performed a null analysis, replacing the patients with normal subjects. We compared the GMC of healthy adult individuals with the mean GMC of the control group. We randomly selected

five healthy adult individuals (mean age, 30 ± 3.9 years) whose images were not used for the construction of the template or control GMC dataset. The images from each one of these individuals were compared with the mean image of the 96 control subjects by using ANCOVA, with age as nuisance factor.

We also were concerned that the differences in GMC between each patient and controls could be an effect of the younger age of some patients, even though all patients, with the exception of one (subject 3), had ages that fell within two SD of the mean age of controls. To address this issue, we randomly selected three normal children (ages 7, 13, and 14 years), and the images from each one of these children were compared with the mean image of the 96 control subjects by using ANCOVA with age as nuisance factor.

RESULTS

Eleven patients were evaluated. Eight patients were submitted to surgical resection of the FCD area, and all of them had the diagnosis of Taylor-type FCD confirmed (3,22). Two patients had neurologic symptoms other than seizures. One patient had a mild left hemiparesis, and another patient exhibited a learning disability.

Each patient had only one area of visually suspected FCD, which was present in a distinct anatomic location for every patient. The location of the visually suspected FCD for each patient is shown in Table 2. Table 2 also displays the results of the VBM analyses, listing the areas of increased GMC for each patient, which are put side by side with the area of visually suspected FCD. The statistical maps of GMC excess of two representative patients are shown in Fig. 1, which displays a comparison between VBM findings and the visual diagnostic MRI results.

Ten (91%) patients showed GMC excess. In nine (82%) patients, visually detected FCD matched the area of significant GMC excess. In seven (64%) patients, GMC excess extended beyond the area of visually detected FCD. Only one patient showed regions of GMC excess that did not overlap the correspondent visually detected FCD.

Among the patients who showed areas of increased GMC, the cluster size of the GMC excess in the region corresponding to the visually detected FCD ranged from 40 to 1,046 mm^3.

Among patients with GMC excess beyond the area of visually suspected FCD, five (71%) had multifocal EEG abnormalities, and five (71%) did not achieve seizure freedom after surgery. Overall, patients who exhibited GMC excess beyond the visually suspected area either showed multifocal EEG, did not achieve seizure control with surgery, or both.

Among patients with other neurologic signs, patient 3, who had mild left hemiparesis, exhibited large visually detected right inferior and middle frontal gyri FCD and VBM abnormalities that encompassed the same locations. Patient 11, who showed learning disabilities, exhibited visually detected right inferior temporal gyrus FCD and pervasive VBM abnormalities involving the right temporal and parietal lobes.

We did not observe a significant difference in GMC between each one of the five randomly selected adult individuals and the control group, or between the three randomly selected children and the control group, by using the same criterion we used for patients, that is, an uncorrected statistical threshold of $p < 0.001$ ($T = 3.18$) with an extent threshold looking for clusters with ≥ 32 contiguous voxels. This finding suggests that the increased GMC observed in patients is due to the presence of FCD, rather than normal variability in sulcal/gyral variability or age effects.

DISCUSSION

We demonstrated that VBM can detect gray-matter abnormalities in a subset of patients with FCD. An optimized VBM protocol was able to detect a significant increase in GMC for almost all patients in the brain areas where FCD was visually diagnosed. This indicates that VBM can detect one of the changes that are associated with FCD, which is an increased thickness of gray matter. Our work supports previous reports that observed a voxel-wise increase in GMC accompanying FCD (27–29). Our study confirms that the increased GMC extends beyond the visually defined FCD (20,28,30). We observed that in the majority of patients from our studied group, VBM detected an increase of GMC that extended beyond the visually diagnosed FCD locations. Even though we do not suggest that VBM should be used as a diagnostic tool for the detection of FCD, we recognize that this finding can be of some importance in improving the understanding of the physiopathology of FCD and its related refractoriness to surgical treatment.

In patients with partial epilepsy due to a cortical dysplastic lesion, FCDs have been conventionally identified by having a neuroimaging expert visually inspect the raw MRI data. Recent techniques have been developed to help neuroradiologists identify regions of FCD (8,31,32). Visual analysis of MRI scans powered by multiplanar and curvilinear reconstruction can substantially improve the detection of FCD (8). Nonetheless, despite the recent advances in the diagnosis of FCD by conventional MRI and postprocessing techniques, neuroimaging methods have previously failed to detect signs of diffuse abnormalities in patients with FCD. Our work suggests that visual inspection may not be sufficient to identify the full extent of the cortical dysplastic lesion in these patients. Our study suggests that patients with FCD can show gray-matter abnormalities detected by a voxel-wise automated statistical morphometric analysis of MRI. These patients exhibit

TABLE 2. *Values of the* t*-statistic ($SPM_{(t)}$) and the values of the* t*-statistic corrected for the normal distribution ($SPM_{(z)}$) depicting the location and the statistical significance of voxels with GMC differences in patients with FCD compared with controls*

		VBM results height threshold: T = 3.18, p = 0.001									
			Voxel					Anatomic location			
Subjects	Visual analysis	Cluster size	T	Equiv Z	X	Y	Z	Hemisphere	Lobe	Location	Brodmann area
Subject 1	Right middle and superior frontal gyri	431	4.12	3.94	15	58	18	Right	Frontal lobe	Superior frontal gyrus	Brodmann area 10
			3.3	3.2	21	50	27				
		32	3.58	3.46	−32	−24	−33	Left	Temporal lobe	Medial occipitotemporal gyrus	Brodmann area 36
		146	3.55	3.43	−41	−28	60		Parietal lobe	Postcentral gyrus	Brodmann area 3
Subject 2	Left inferior parietal lobule	6152	4.79	4.52	−8	−69	53	Left	Parietal lobe	Precuneus	Brodmann area 7
			4.48	4.26	−11	−45	56				
			4.19	4	−5	−52	57				
		205	4.3	4.1	−47	−31	−31		Temporal lobe	Fusiform gyrus	Brodmann area 20
		326	4.23	4.03	11	−65	42	Right	Parietal lobe	Precuneus	Brodmann area 7
		482	3.93	3.77	−35	−49	60	Left		Superior parietal lobule	
		155	3.79	3.64	−61	−28	40			Postcentral gyrus	Brodmann area 2
		271	3.53	3.41	−61	−59	27		Temporal lobe	Superior temporal gyrus	Brodmann area 39
			3.51	3.39	−63	−48	30		Parietal lobe	Supramarginal gyrus	Brodmann area 40
			3.5	3.38	−63	−44	39			Inferior parietal lobule	
		43	3.49	3.38	−60	6	23		Frontal lobe	Inferior frontal gyrus	Brodmann area 9
		33	3.32	3.22	−9	−79	24		Occipital lobe	Cuneus	Brodmann area 18
		32	3.3	3.2	−46	−60	34		Parietal lobe	Angular gyrus	Brodmann area 39
Subject 3	Right inferior and middle frontal gyri	1046	4.58	4.34	38	38	−4	Right	Frontal lobe	Middle frontal gyrus	Brodmann area 47
			4.11	3.93	23	43	−12				Brodmann area 11
			3.68	3.55	19	37	−19			Inferior frontal gyrus	
		71	3.79	3.64	9	45	−22	Right	Frontal lobe	Rectal gyrus	
		57	3.39	3.28	−29	−60	55	Left	Parietal lobe	Superior parietal lobule	Brodmann area 7
Subject 4	Left superior frontal gyrus	2506	4.42	4.2	−23	−82	34	Left	Occipital lobe	Cuneus	Brodmann area 19
			4.4	4.18	−25	−79	42		Parietal lobe	Precuneus	
		700	4.21	4.02	21	−89	16	Right	Occipital lobe	Middle occipital gyrus	Brodmann area 18
			3.59	3.46	23	−85	32			Cuneus	Brodmann area 19
		92	3.77	3.62	−20	47	32	Left	Frontal lobe	Superior frontal gyrus	Brodmann area 9
		100	3.72	3.58	−40	−71	20		Occipital lobe	Transoccipital sulcus	Brodmann area 19
		103	3.41	3.3	−4	−74	51			Precuneus	Brodmann area 7
Subject 5	Right superior frontal gyrus	612	5.3	4.94	12	59	15	Right	Frontal lobe	Superior frontal gyrus	Brodmann area 10
Subject 6	Right postcentral gyrus	720	4.39	4.17	−67	−28	14	Left	Temporal lobe	Superior temporal gyrus	Brodmann area 42
			3.49	3.37	−66	−30	26		Parietal lobe	Inferior parietal lobule	Brodmann area 40
			3.35	3.25	−63	−28	7		Temporal lobe	Superior temporal gyrus	Brodmann area 42
		172	3.81	3.66	64	−24	9	Right			
		240	3.73	3.59	−63	−42	40	Left	Parietal lobe	Inferior parietal lobule	Brodmann area 40
			3.41	3.3	−58	−46	48				
		193	3.67	3.54	−42	−50	57				
		120	3.66	3.53	11	−55	−31	Right	Cerebellum	Peduncle	
		379	3.63	3.5	61	−33	26		Parietal lobe	Inferior parietal lobule	Brodmann area 40
			3.22	3.13	62	−25	22			Postcentral gyrus	
		577	3.57	3.45	36	−92	−1		Occipital lobe	Inferior occipital gyrus	Brodmann area 18
			3.48	3.37	26	−94	5			Middle occipital gyrus	

TABLE 2. *Continued.*

		VBM results height threshold: T = 3.18, p = 0.001								
				Voxel				Anatomic location			
Subjects	Visual analysis	Cluster size	T	Equiv Z	X	Y	Z	Hemisphere	Lobe	Location	Brodmann area
		61	3.55	3.43	−52	−69	37	Left	Parietal lobe	Angular gyrus	Brodmann area 39
		44	3.55	3.43	27	−25	−9	Right	Temporal lobe	Subgyral	Hippocampus
		185	3.55	3.43	−9	−53	−27		Cerebellum	Peduncle	
		192	3.53	3.41	23	55	4	Right	Frontal lobe	Superior frontal gyrus	Brodmann area 10
		35	3.37	3.26	−48	32	7	Left	Frontal lobe	Inferior frontal gyrus	Brodmann area 46
Subject 7	Left cingulate gyrus	292	3.82	3.68	−57	−32	29	Left	Parietal lobe	Inferior parietal lobule	Brodmann area 40
		40	3.73	3.59	−3	−13	30		Limbic lobe	Cingulate gyrus	Brodmann area 23
Subject 8	Right precentral sulcus	145	4.29	4.09	−27	−75	25	Left	Occipital lobe	Precuneus	Brodmann area 31
Subject 9	Right precentral gyrus	55	5.03	4.72	48	−5	35	Right	Frontal lobe	Precentral gyrus	Brodmann area 6
Subject 11	Right inferior temporal gyrus	1604	6.54	5.92	34	−27	−9	Right	Temporal lobe	Subgyral	Hippocampus
			3.76	3.62	36	−12	−20				Brodmann area 20
		74	4.01	3.84	49	−15	21		Parietal lobe	Postcentral gyrus	Brodmann area 43
		147	3.71	3.58	39	−27	−31		Temporal lobe	Inferior temporal gyrus	Brodmann area 20
		138	3.63	3.5	23	−22	−28		Limbic lobe	Parahippocampal gyrus	Brodmann area 36
		34	3.32	3.22	49	−6	−4		Temporal lobe	Superior temporal gyrus	Brodmann area 22

The anatomic location of the areas with GMC difference is described together with the stereotaxic coordinates. SPM, statistical parametric mapping; GMC, gray-matter concentration; FCD, focal cortical dysplasia

a focal increased GMC, compared with normal controls. The areas of GMC are not exclusively located at the region of suspected FCD and may represent dysplastic features conspicuously distributed. The group of patients studied falls into the category that has been defined as Taylor-type FCD (dysmorphic neurons without or with balloon cells) by Palmini et al. (22). That explains why they had visually defined MRI abnormalities, because the type I (no dysmorphic neurons or balloon cells) is probably not detected by current diagnostic MRI techniques. These patients correspond to the most severe spectrum of FCD abnormalities (and hence had visual diagnosis of FCD), which can explain the fact that we observed clear-cut VBM results on the site of visually defined FCD. However, those areas not visually defined as abnormal, but detected as such by VBM, could possibly correspond to type I or mild malformations of cortical development, which possibly exemplifies the spectrum of abnormalities in patients with FCD.

Altogether, the areas of increased GMC in these patients may contribute to the origin and maintenance of seizures. This finding supports the notion that the surgical refractoriness observed in patients with FCD can be due to the incomplete resection of the dysplastic tissue.

It is noteworthy that, in some patients, VBM detected scattered increased GMC across over more than one cerebral lobe. Combining clinical, EEG, and surgical information, it is possible to infer that these areas are probably abnormal dysplastic tissue. All patients who had VBM abnormalities encompassing more than one cerebral lobe also had multifocal EEG activity (independent ictal or interictal epileptiform discharges in two or more different cerebral lobes), with the exception of two patients (numbers 2 and 4). Nonetheless, patients 2 and 4 did not achieve seizure freedom after surgery (Table 1). In addition, both patients with neurologic manifestations other than seizures (subjects 3 and 11) did exhibit pervasive VBM abnormalities. Patient 3 showed a left hemiparesis that was compatible with an extensive left precentral dysplasia, whereas patient 11 exhibited learning disability and pervasive temporal and parietal abnormalities. We believe that the combination of clinical, EEG, and postoperative data in our group of patients corroborates the potential epileptogenic nature of the abnormalities detected by VBM. All patients with VBM abnormalities extending beyond the visually detected area either showed multifocal EEG or were refractory to surgical treatment.

In addition, we failed to observe GMC abnormalities when normal subjects, including children, were compared with control subjects. This indicates that the abnormalities seen in patients with FCD are unlikely to be due to normal individual variability of sulci and gyri distribution or to age effects of gray-matter distribution.

Our extensive attempts to minimize false alarms necessarily imply low statistical power. Therefore the true tissue

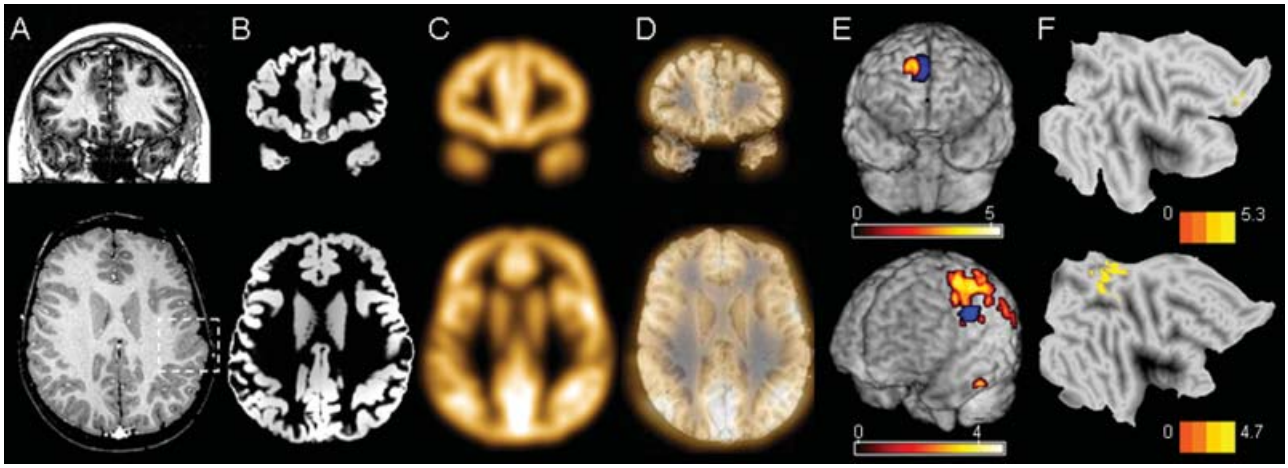

FIG. 1. Data from two representative patients with voxel-based morphometry (VBM) results matching the location of the visually suspected FCD and the process of GMC analysis. The left column **(A)** shows the slice of the T_1-weighted MRI scan in which the suspected lesion is highlighted (dotted line square). **B:** Probabilistic map of distribution of gray matter. **C:** Map of gray matter smoothed with 10-mm kernel that is applied with the purpose of minimizing interindividual sulci and gyri differences. **D:** Overlay of the smoothed map of gray matter and the structural scan. **E:** Three-dimensional reconstruction of the patient's brain, with a double overlay composed by the VBM statistical map of increased GMC (in a red–yellow color gradient with a corresponding Z-score scale bar) and the region of the visually suspected FCD drawn in blue. **F:** Extent of the statistical map of increased GMC, which is overlaid on a flat-map template of the cortical mantle (35). The **top row** displays the data from subject 5, who exhibited an FCD located in the right superior frontal gyrus. In this patient, the regions of VBM-detected increased GMC did not extend far beyond the visually detected area of FCD. **Bottom row:** Data from subject 2, who exhibited a visually suspected FCD lesion on the inferior parietal lobule. In this patient, the statistical map of increased GMC matched the location of the visually defined FCD, but also extended beyond it, encompassing areas that did not appear abnormal in the diagnostic MRI.

abnormality may be more extensive than suggested by our analysis. For example, we attempted to account for age by using ANCOVA, which may be much more conservative than conducting an analysis using an age-matched control group. Furthermore, our conservative statistical threshold of $p < 0.001$ reduces our ability to detect abnormalities. Unlike MTLE (in which a common pattern of GMC abnormalities appears to be present across individuals), FCD clearly influences different cortical regions across individuals. This individual variability requires single-subject analyses, which can considerably reduce statistical power.

Our present study demonstrates that VBM can be useful for investigating FCD. Our results support findings from other centers, which reported a high rate of FCD detection by using automated VBM techniques [12 correct detections in 17 patients, according to the work of Srivastava et al. (33), and 21 of 27 patients according to the work of Colliot et al. (28)]. Therefore it appears that VBM is sensitive in detecting brain abnormalities in patients with FCD. Nonetheless, we suggest that VBM results should be interpreted with caution. For example, our optimized VBM protocol (with a custom template tuned for our scanner as well as local demographics) may be more sensitive than conventional VBM.

Furthermore, VBM may not be accurate enough to be used as a preoperative planning tool for the treatment of FCD. Even though we showed that VBM can identify increased GMC in areas of FCD, we have not established the clinical reliability of this technique (e.g., we have no histologic evidence that the areas identified as abnormal by VBM that appeared normal on visual inspection are indeed dysplastic). However, our work does suggest that FCD often results from a more dispersed lesion than those observed by simple visual inspection of MRI scans. In any case, regions identified by VBM may warrant more careful monitoring or examination with conventional techniques such as visual inspection combined with EEG. Alternatively, VBM results could be used to guide high-resolution MRI scans of the suspected regions (e.g., regions revealed by whole-brain VBM could be investigated by using a high-resolution surface coil with a restricted field of view).

One problem associated with using VBM to investigate FCD lies with the techniques used for segmenting of brain tissues. Defining three tissue types (CSF and gray and white matter) relies on the clear-cut distinction of these healthy tissues. VBM has been successfully used in the past to offer information regarding the distribution of gray and white matter, but usually when the features of the tissue are broadly preserved and the changing factor is the concentration or volume of the tissues. In our present study, we used a standard method for segmenting brain tissues only optimized by the use of gray-matter priors from a custom template (e.g., the template image is tuned for our scanner). We observed that the pathologic FCD region is typically classified as an increased volume or concentration of GMC. However, histologic studies demonstrate that FCD also can occur as a disorganized architecture of the cortical layers without any alteration of the thickness of the cortical mantle (34). This aspect of FCD is most likely missed by VBM. However, texture-based analysis of the

cortex of patients with FCD has suggested that these lesions can be detected by automated texture-extraction neuroimaging routines (32) as well. The sensibility of VBM in the detection of FCD is probably hampered by the fact that only one aspect of the FCD is detected, the increased cortical thickness or density. We suggest that the detection of FCD by using automated neuroimaging techniques can have their sensibility and specificity improved if VBM is combined with other tools that could identify alterations in the organization of the cortical mantle. In that respect, the combination of texture analysis and VBM is particularly promising and should be addressed by further studies. In summary, our research offers a proof of concept, clearly illustrating that automated analysis of MRI scans can reveal abnormalities missed by visual inspection. However, reliable clinical applications would probably benefit from a more complex method of segmentation (detecting abnormal texture or structure, instead of simply assuming that all brain regions are healthy white matter, healthy gray matter, or CSF).

Acknowledgment: This study was supported by FAPESP (00/04710-2).

REFERENCES

1. Montenegro MA. Focal cortical dysplasia. *Arch Neurol* 2003;60:634–636.
2. Kral T, Clusmann H, Blumcke I, et al. Outcome of epilepsy surgery in focal cortical dysplasia. *J Neurol Neurosurg Psychiatry* 2003;74:183–188.
3. Taylor DC, Falconer MA, Bruton CJ, et al. Focal dysplasia of the cerebral cortex in epilepsy. *J Neurol Neurosurg Psychiatry* 1971;34:369–387.
4. Engel J Jr. *Surgical treatment of the epilepsies*. New York: Raven Press, 1987.
5. Jackson GD. New techniques in magnetic resonance and epilepsy. [Review]. *Epilepsia* 1994;35(suppl 6):S2–S13.
6. Barkovich AJ, Kuzniecky RI, Jackson GD, et al. Classification system for malformations of cortical development: update 2001. *Neurology* 2001;57:2168–2178.
7. Montenegro MA, Guerreiro MM, Lopes-Cendes S, et al. Relevance of genetic and prenatal events in different forms of malformations of cortical development. *Neurology* 2001;56:A135.
8. Montenegro MA, Li LM, Guerreiro MM, et al. Focal cortical dysplasia: improving diagnosis and localization with magnetic resonance imaging multiplanar and curvilinear reconstruction. *J Neuroimaging* 2002;12:224–230.
9. Kloss S, Pieper T, Pannek H, et al. Epilepsy surgery in children with focal cortical dysplasia (FCD): results of long-term seizure outcome. *Neuropediatrics* 2002;33:21–26.
10. Cohen-Gadol AA, Ozduman K, Bronen RA, et al. Long-term outcome after epilepsy surgery for focal cortical dysplasia. *J Neurosurg* 2004;101:55–65.
11. Chung CK, Lee SK, Kim KJ. Surgical outcome of epilepsy caused by cortical dysplasia. *Epilepsia* 2005;46(suppl 1):25–29.
12. Frater JL, Prayson RA, Morris HH III, et al. Surgical pathologic findings of extratemporal-based intractable epilepsy: a study of 133 consecutive resections. *Arch Pathol Lab Med* 2000;124:545–549.
13. Gomez-Anson B, Thom M, Moran N, et al. Imaging and radiological-pathological correlation in histologically proven cases of focal cortical dysplasia and other glial and neuronoglial malformative lesions in adults. *Neuroradiology* 2000;42:157–167.
14. Prayson RA, Estes ML. Cortical dysplasia: a histopathologic study of 52 cases of partial lobectomy in patients with epilepsy. *Hum Pathol* 1995;26:493–500.
15. Taylor DC, Falconer MA, Bruton CJ, et al. Focal dysplasia of the cerebral cortex in epilepsy. *J Neurol Neurosurg Psychiatry* 1971;34:369–387.
16. Prayson RA, Spreafico R, Vinters HV. Pathologic characteristics of the cortical dysplasias. *Neurosurg Clin North Am* 2002;13:17–25, vii.
17. Palmini A, Gambardella A, Andermann F, et al. Intrinsic epileptogenicity of human dysplastic cortex as suggested by corticography and surgical results. *Ann Neurol* 1995;37:476–487.
18. Friston KJ, Holmes AP, Worsley K, et al. Statistic parametric maps in functional imaging: a general linear approach. *Hum Brain Mapp* 1995;2:189–210.
19. Bonilha L, Kobayashi E, Rorden C, et al. Medial temporal lobe atrophy in patients with refractory temporal lobe epilepsy. *J Neurol Neurosurg Psychiatry* 2003;74:1627–1630.
20. Bonilha L, Rorden C, Castellano G, et al. Voxel-based morphometry of the thalamus in patients with refractory medial temporal lobe epilepsy. *Neuroimage* 2005;25:1016–1021.
21. Bonilha L, Rorden C, Castellano G, et al. Voxel-based morphometry reveals gray matter network atrophy in refractory medial temporal lobe epilepsy. *Arch Neurol* 2004;61:1379–1384.
22. Palmini A, Najm I, Avanzini G, et al. Terminology and classification of the cortical dysplasias. *Neurology* 2004;62:S2–S8.
23. Commission on Classification and Terminology of the International League Against Epilepsy. Proposal for revised classification of epilepsies and epileptic syndromes. *Epilepsia* 1989;30:389–399.
24. Colombo N, Tassi L, Galli C, et al. Focal cortical dysplasias: MR imaging, histopathologic, and clinical correlations in surgically treated patients with epilepsy. *AJNR Am J Neuroradiol* 2003;24:724–733.
25. Rorden C, Brett M. Stereotaxic display of brain lesions. *Behav Neurol* 2000;12:191–200.
26. Good CD, Johnsrude IS, Ashburner J, et al. A voxel-based morphometric study of ageing in 465 normal adult human brains. *Neuroimage* 2001;14:21–36.
27. Richardson MP, Friston KJ, Sisodiya SM, et al. Cortical grey matter and benzodiazepine receptors in malformations of cortical development. a voxel-based comparison of structural and functional imaging data. *Brain* 1997;120:1961–1973.
28. Colliot O, Bernasconi N, Khalili N, et al. Individual voxel-based analysis of gray matter in focal cortical dysplasia. *Neuroimage* 2005; [Epub ahead of print].
29. Wilke M, Kassubek J, Ziyeh S, et al. Automated detection of gray matter malformations using optimized voxel-based morphometry: a systematic approach. *Neuroimage* 2003;20:330–343.
30. Sisodiya SM, Free SL, Stevens JM, et al. Widespread cerebral structural changes in patients with cortical dysgenesis and epilepsy. *Brain* 1995;1184:1039–1050.
31. Antel SB, Bernasconi A, Bernasconi N, et al. Computational models of MRI characteristics of focal cortical dysplasia improve lesion detection. *Neuroimage* 2002;17:1755–1760.
32. Bernasconi A, Antel SB, Collins DL, et al. Texture analysis and morphological processing of magnetic resonance imaging assist detection of focal cortical dysplasia in extra-temporal partial epilepsy. *Ann Neurol* 2001;49:770–775.
33. Srivastava S, Maes F, Vandermeulen D, et al. Feature-based statistical analysis of structural MR data for automatic detection of focal cortical dysplastic lesions. *Neuroimage* 2005;27:253–266.
34. Sisodiya SM. Malformations of cortical development: burdens and insights from important causes of human epilepsy. *Lancet Neurol* 2004;3:29–38.
35. Van Essen DC, Drury HA, Dickson J, et al. An integrated software suite for surface-based analyses of cerebral cortex. *J.Am Med Inform Assoc* 2001;8:443–459.